Non-line-of-sight underwater optical wireless communication network

Shlomi Arnon[1,*] and Debbie Kedar[1]

[1]*Satellite and Wireless Communications Laboratory, Electrical and Computer Engineering Department, Ben-Gurion University of the Negev, P O Box 653, IL-84105 Beer-Sheva, Israel*
**Corresponding author: shlomi@ee.bgu.ac.il*

Received September 3, 2008; revised November 21, 2008; accepted December 30, 2008; posted January 12, 2009 (Doc. ID 101024); published February 12, 2009

The growing need for ocean observation systems has stimulated considerable interest within the research community in advancing the enabling technologies of underwater wireless communication and underwater sensor networks. Sensors and *ad hoc* sensor networks are the emerging tools for performing extensive data-gathering operations on land, and solutions in the subsea setting are being sought. Efficient communication from the sensors and within the network is critical, but the underwater environment is extremely challenging. Addressing the special features of underwater wireless communication in sensor networks, we propose a novel non-line-of-sight network concept in which the link is implemented by means of back-reflection of the propagating optic signal at the ocean-air interface and derive a mathematical model of the channel. Point-to-multipoint links can be achieved in an energy efficient manner and broadcast broadband communications, such as video transmissions, can be executed. We show achievable bit error rates as a function of sensor node separation and demonstrate the feasibility of this concept using state-of-the-art silicon photomultiplier detectors.

OCIS codes: 010.0280, 010.4450, 040.3780, 040.5250, 060.2605, 060.4510.

1. INTRODUCTION

Gathering data from the ocean has been of interest to man for many years for the purposes of scientific research as well as for pollution monitoring, seismic studies, and oil and gas pipeline maintenance and security [1–3]. Existing underwater sensors are expensive, and their deployment and recovery can be extremely costly, reaching as much as $25,000 per day for the use of a deep-ocean ship [4]. Commonly, these sensors are distributed sparsely over the area of interest and retrieved infrequently for data harvesting or, alternatively, attached to autonomous underwater vehicles affording high mobility and flexibility in deployment and data assimilation, but also incurring delay in data retrieval and expense. However, there are many emerging applications, such as security, surveillance, and oil pipeline monitoring, where fine-grained data profiles are needed in real time and, sometimes, around the clock. Wireless sensor networks (WSN) are providing this kind of rich data in numerous terrestrial applications, and there is now growing interest in investigating the potential of underwater WSN [3–6]. Heidemann *et al.* propose a system solution for seismic monitoring of offshore oilfields and address many network- and datalink-level issues for short-range communications.

Partan *et al.* underline some of the major differences between terrestrial and underwater wireless sensor networks and raise the question of defining different metrics for underwater applications, where equipment and deployment are major expenses making operational energy budgets less critical despite problems of onboard sensor battery power. Akyildiz *et al.* have extensively reviewed work done in underwater acoustic networks and highlighted research challenges. They envisage a tiered architecture with a hybrid communication model using above-water gateways.

Currently, research is being carried out on a number of levels, from the design of robust, low-cost sensors to the development of tailored communication protocols that address the special needs of underwater networking [7,8]. Experimental work has been reported [7,9] demonstrating practical solutions to issues of sensor node orientation, waterproofing, biofouling protection, and localization. The object of this paper is to focus on issues of the wireless communication link at the physical layer, and we propose a novel non-line-of-sight (NLOS) optical solution with unique features.

Acoustic communication is the widespread method for underwater wireless communication, and ranges of hundreds of kilometers can be attained. However, data rates are restricted because of severe, frequency-dependent attenuation and surface-induced pulse-spread from reflection. Data rates of ≈20 kbs have been achieved for ranges of a kilometer in deep ocean and ≈300–500 bps for ranges of up to 100 km in shallow water and 200 km in deep ocean [6]. The speed of acoustic waves in the ocean is ≈1500 m/s so that long-range communications involve high latency that poses a problem for synchronization and multiple access protocols. In practice most acoustic links operate in half-duplex mode and, within a sensor network, sensor-to-sensor communication is an unsolved issue restricting network topologies to star configurations with a base station at the hub. Time-varying multipath interference, shadow zones, bubble-cloud attenuation

near the surface, and potential harm to marine mammals are further concerns associated with underwater acoustic wireless communication.

In view of these limitations, optical wireless communication, also termed free space optics (FSO), is a promising alternative for underwater links within a sensor network. Although the high data rates characteristic of terrestrial and space FSO are threatened by extremely high absorption and scattering there is evidence that broadband links can be achieved over moderate ranges. Hanson and Radic [10] demonstrated 1 Gbs transmissions in a laboratory experiment with a simulated aquatic medium with scattering characteristics similar to oceanic waters. They expanded their study using Monte Carlo simulations to predict longer-range underwater FSO performance with bandwidths over 5 GHz for a range of 64 m in clear ocean water, dropping to 1 GHz for a range of 8 m in turbid harbor water. Demonstrations of oceanic FSO over ranges of $\approx$100 m using a LED transmitter are cited [11]. Detweiller, Vasilescu and Rus [7] describe experimental work on an underwater sensor network with hybrid acoustic-optical wireless communication links, benefiting from the broadcast facility of the acoustic technology and the high data rates afforded by an optical point-to-point link. However, when sensors are deployed on the seabed or maintained at a near-fixed depth by buoyancy control, line-of-sight (LOS) may not be achievable or may be obstructed by floating platform infrastructure, etc.

In this paper we investigate an innovative sensor network concept based on FSO with broadband capacity that could be scalable. Transmission range restrictions are overcome by virtue of multiple hops, and reliable network operation with no single point of failure or bottleneck is provided by the broadcast nature of the transmission and redundancy in the sensor dispersal. Pivotal to the concept developed in this paper is the idea of non-line-of-sight (NLOS) communication. We have presented an outline of a terrestrial NLOS optical wireless sensor network wherein backscattering of light by molecules and aerosols in the atmosphere functions as a vehicle of communication in a similar way to the deployment of numerous tiny reflecting mirrors [12], and we have examined multiple access challenges and solutions in this context [13]. In the current work we extend this concept to the underwater environment, where the reflection is actuated by the ocean–air surface, and evaluate the system feasibility with a numerical example. In [14] we explored the feasibility of an underwater optical oceanic probing scheme and reviewed the optical properties of the ocean that are fundamental to the achievement of an operable sensor network.

In Section 2 we will briefly expand on the properties of the ocean relevant to FSO. In Section 3 we develop the mathematical models for assessing the system link budget. In Section 4 we present the bit error rate (BER) calculation, and in Section 5 we evaluate system performance with a numerical example. In Section 6 we discuss and summarize the results and draw conclusions. The preliminary study provides insight into the potential communication performance of a single node-to-node link, although much further work is needed to model the complex oceanic surface and light–water interactions such as multiple scattering and solar radiance transmission.

2. OCEANIC CHANNEL PROPERTIES

Light propagation in seawater is highly wavelength sensitive, with transmittance falling from near 100% over several meters in clear ocean water for light of wavelengths 400–500 nm to near zero for turbid waters and wavelengths below 300 nm and above 700 nm [15,16]. This is due to the spectral dependence of scattering and absorption caused by aquatic molecules and suspended particles. These properties display high variability that is depth dependent (up to an order of magnitude) as well as varying over time because of changing oceanic composition and prevailing weather [17]. For the purpose of this work we shall adopt, as typical figures, the values used in [10] (see Table 1). These were based on the findings recorded in [18] for absorption and scattering coefficients $\alpha(\lambda)$ and $\beta(\lambda)$, respectively, from measurements made in the spectral band centered at 530 nm. The total attenuation is described by the extinction coefficient $c(\lambda)$, which is related to $\alpha(\lambda)$ and $\beta(\lambda)$ by the simple expression

$$c(\lambda) = \alpha(\lambda) + \beta(\lambda). \tag{1}$$

It is clear from any text on ocean optics that attributing a single value to the extinction coefficient at a given wavelength is a gross oversimplification, and we note that the preferred wavelength for superior transmission of an optic signal ranges between 400 nm and 550 nm depending on the precise water composition.

In a multiple scattering channel the optic power arriving at the receiver is not only depleted by absorption and light scattered out of the propagating beam, but also augmented by light scattered back into the beam after several scattering events. The precise nature of light reception in these circumstances requires a detailed model of the scattering properties of the medium and is not a trivial issue. The additional received light that has been multiply scattered results in pulse stretching in the time domain. We envisage a gated receiver scheme as will be described in Section 4 and so do not consider the later arriving multiply scattered optic power.

When light propagating through a medium encounters an interface between areas of different refractive indices it is partially transmitted (refracted) and partially reflected in accordance with Fresnel's law for dielectric media and Snell's law of refraction. To predict the behavior of light at the ocean–air surface it is necessary to ascertain the value of the seawater refractive index, which is dependent on the water temperature and salinity. The fol-

Table 1. Hermite Polynomials of Order *n*

n	$H_n(\eta)$
0	1
1	η
2	η^2-1
3	$\eta^3-3\eta$
4	$\eta^4-6\eta^2+3$

lowing model has recently been proposed for the approximation of the refractive index of seawater n_w and is valid for temperatures in the range $0\,^{\circ}\mathrm{C} < \mathrm{Temp} < 30\,^{\circ}\mathrm{C}$, salinities in the range $0\% < S < 35\%$, and optical wavelengths in the range $400 < \lambda < 700$ nm [19]:

$$n_w(S,\mathrm{Temp},\lambda) = n_0 + (n_1 + n_2\mathrm{Temp} + n_3\mathrm{Temp}^2)S + n_4\mathrm{Temp}^2 + \frac{n_5 + n_6 S + n_7\mathrm{Temp}}{\lambda} + \frac{n_8}{\lambda^2} + \frac{n_9}{\lambda^3}, \quad (2)$$

where n_0 to n_9 are empirically verified constants. The values obtained vary from 1.32913 for $\mathrm{Temp}=30\,^{\circ}\mathrm{C}$, $S=0\%$, $\lambda=700$ nm to 1.35093 for $\mathrm{Temp}=1\,^{\circ}\mathrm{C}$, $S=34.998\%$, $\lambda=404.7$ nm.

Considerable work has been devoted to studying the reflection of light from the atmosphere (primarily sunlight) by the sea surface, where sun zenith angle and wind speed are dominant factors. However, the reflection of light from underwater at the ocean–air surface, which is central to the NLOS communication concept, has scarcely been investigated to the best of the authors's knowledge. Since the refractive index of air is lower than that of water, some incident skylight will always penetrate the sea and comprise a source of background illumination contaminating a propagating underwater optical signal. This will vary greatly with depth, receiver parameters (field-of-view, pointing direction, filter bandwidth, etc.), and ambient conditions (sun zenith angle, season, latitude, atmospheric conditions, etc.) but is not considered in this paper because of the assumptions detailed in Section 4.

In the reverse direction the opposite is the case and, above a critical incidence angle, total internal reflection (TIR) can be achieved as explained in Section 3. Nevertheless, the reflecting surface has the same three-dimensional contour regardless of the incident direction of the light of interest, and the geometry of this surface must be modeled if we wish to calculate the propagation parameters of an optic signal. Sea surface height is measured in the time domain at different locations around the globe using buoys with accelerometers or magnetometers [20,21], and is commonly considered to be Gaussian or Rayleigh in distribution [22,23]. Furthermore, the sea surface slope, which is of interest in this work since it determines the reflection angles of incident light, is also widely considered to be Gaussian as a first-order approximation [24], while the parameter characterizing sea "roughness" and consequent variance in surface slope is the wind speed and direction variation. In the limit, the sea surface has been modeled as a plane surface bounding a semi-infinite dielectric medium and surface emissivity has been calculated accordingly [24].

3. COMMUNICATION SYSTEM LINK BUDGET

In this section we develop the mathematical expressions with which we can derive the performance of the proposed system.

A. LOS Communication Link

The common FSO link in optical wireless communication systems between two points is a LOS link as illustrated in Fig. 1. The optical signal reaching the receiver is obtained by multiplying the transmitter power, telescope gain, and losses, and is given by [25] as

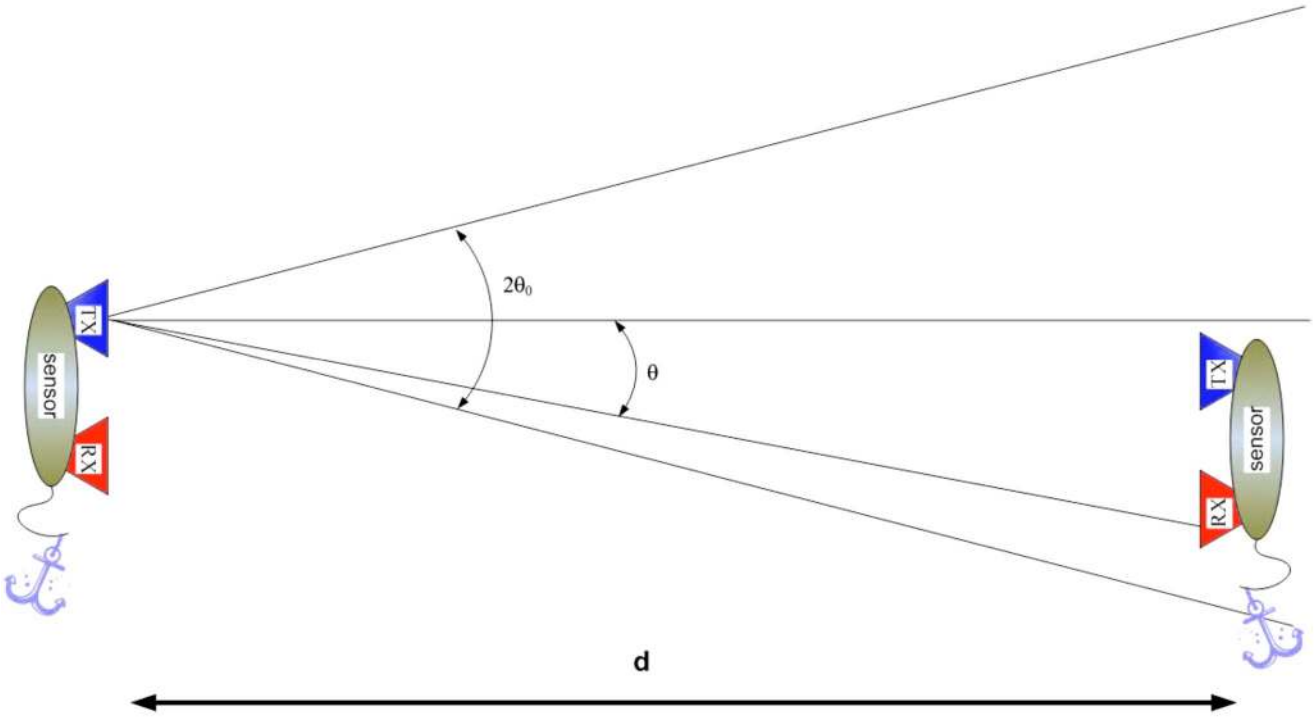

Fig. 1. (Color online) Line-of-sight (LOS) communication scenario.

$$P_{R\_los} = P_T \eta_T \eta_R \exp\left[-c(\lambda)\frac{d}{\cos(\theta)}\right]\frac{A_{\mathrm{Rec}}\cos(\theta)}{2\pi d^2[1-\cos(\theta_0)]}, \quad (3)$$

where P_T is the average transmitter optical power, η_T is the optical efficiency of the transmitter, η_R is the optical efficiency of the receiver, d is the perpendicular distance between the transmitter and the receiver plane, θ is the angle between the perpendicular to the receiver plane and the transmitter-receiver trajectory, A_{Rec} is the receiver aperture area, and θ_0 is the laser beam divergence angle.

B. Reflective Communication Link

In some communication scenarios LOS is not available due to obstructions, misalignment, or random orientation of the transceivers. This would be a common circumstance for underwater sensor nodes or in the case of mobile users and leads us to propose an inventive method for achieving a communication link. In addition, the proposed method affords the advantages of point-to-multipoint links and hence facilitates broadcast communication. The fundamental idea of reflective communication is illustrated in Fig. 2. The laser transmitter emits a cone of light defined by inner and outer angles $\theta_{\min}$ and $\theta_{\max}$ in the upward direction. We assume that the sensor nodes self align so that the transmitter faces vertically upward at all times. The light reaching the ocean–air surface illuminates an annular area and is partially bounced back in accordance with the reflectivity property described below.

At an interface between areas of different refractive indices, propagating light is partially transmitted (refracted) and partially reflected in accordance with Fresnel's law for dielectric media. If the light is polarized with the electric field of the light perpendicular to the plane of the diagram above (s-polarized), the reflection coefficient is given by

$$R_s = \left[\frac{n_W\cos(\theta_i) - n_A\cos(\theta_t)}{n_W\cos(\theta_i) + n_A\cos(\theta_t)}\right]^2 = \left[\frac{\sin(\theta_i - \theta_t)}{\sin(\theta_i + \theta_t)}\right]^2, \quad (4)$$

where θ_i and θ_t are the angles of incidence and of transmission (the latter is derived from the former using Snell's Law) and n_A is the refractive index of air.

If the incident light is polarized in the plane of the diagram (p-polarized), the reflection coefficient is given by

$$R_s = \left[\frac{n_W\cos(\theta_t) - n_A\cos(\theta_i)}{n_W\cos(\theta_t) + n_A\cos(\theta_i)}\right]^2 = \left[\frac{\tan(\theta_t - \theta_i)}{\tan(\theta_t + \theta_i)}\right]^2. \quad (5)$$

The respective transmission coefficients are given by $T_s = 1 - R_s$ and $T_p = 1 - R_p$.

Polarized light propagating through an aquatic channel would loose its polarization properties due to the scattering nature of the medium, so that we can assume that the light reaching the ocean–air surface is totally unpolarized and its reflectivity is then given by $R = \frac{1}{2}(R_s + R_p)$.

When the refractive index in the incident medium is higher than in the second medium, as with an underwater optic signal reaching the ocean–air surface, then, if the angle of incidence surpasses a critical value, TIR occurs and all the light will be reflected back as if the interface were a perfect mirror. The critical angle is given by

$$\theta_c = \sin^{-1}\left(\frac{n_A}{n_W}\right). \quad (6)$$

Reflectivity as a function of incidence angle for the data in Table 1 is shown in Fig. 3.

We propose to use the TIR phenomenon to achieve an effective communication channel. If $\theta_{\min} < \theta_c$ then TIR will not be achieved and only some of the light will be reflected back in accordance with Fig. 3. However, the optic path, and consequent attenuation, of light reflected at $\theta_{\min} < \theta < \theta_c$ is shorter than for $\theta_c < \theta < \theta_{\max}$, so that at depth x below the ocean–air surface the light intensity distribution received by the receiver will be a complicated interplay of reflectivity and attenuation.

C. Reflective Channel with a Wavy Surface

In this section we add the effect of the waviness of the sea surface. The seminal works of Cox and Munk in the 1950s revealed the very-near Gaussian probability distribution function (pdf) of the slope, and several works published since then have confirmed and extended these results [26–28]. In those works the authors computed a Gram–

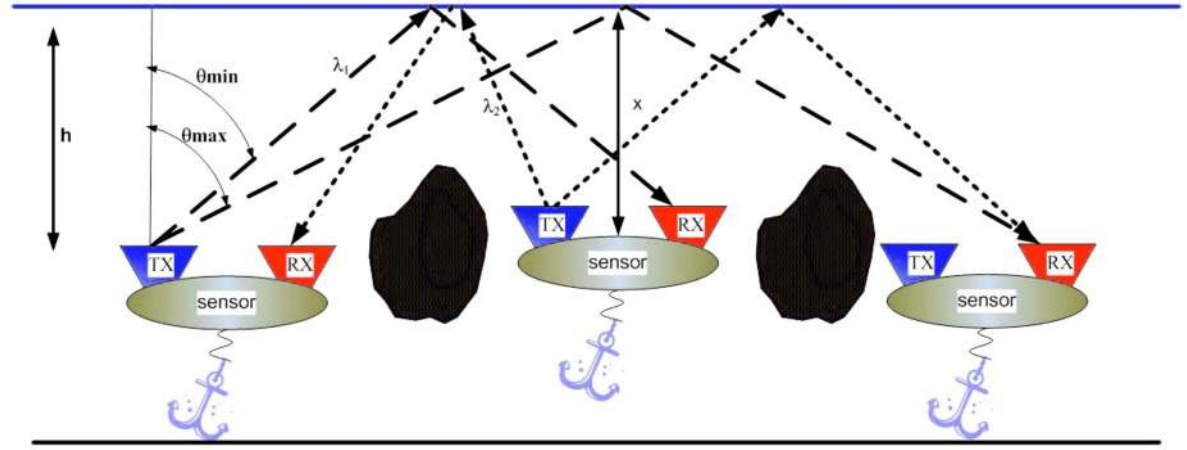

Fig. 2. (Color online) Reflective communication scenario.

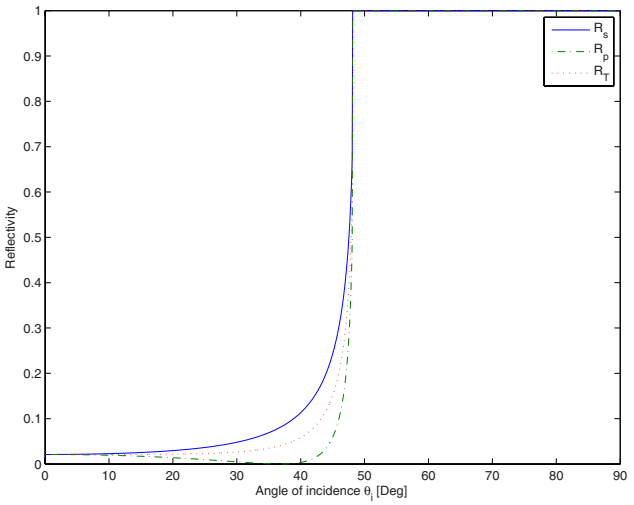

Fig. 3. (Color online) Graph showing reflectivity at the ocean–air surface as a function of incidence angle θ_i using parameters in Table 2.

Charlier series of approximate Gaussian distribution in order to obtain an analytical model for the wave slope density distribution function that would accurately correspond to measured sea surface contours. The basic expression for the slope pdf using the Gram–Charlier series is given by

$$p(\eta) = \sum_{n=0}^{N} \left(\frac{c_n}{n!}\right) H_n(\eta) \frac{1}{\sqrt{2\pi}} \exp\left(-\frac{\eta^2}{2}\right), \tag{7}$$

where η is the normalized slope, c_n are expansion coefficients, and $H_n(\eta)$ are the nth-order Hermite polynomials listed in Table 1. The normalized slope is given by

$$\eta = \frac{\delta - \bar{\delta}}{\sigma_{\text{slope}}}, \tag{8}$$

where δ is the slope angle with respect to nadir, $\bar{\delta}$ is the mean slope angle, and σ_{slope} is the standard deviation.

The wave slope pdf obtained from experimental data differs from the Gaussian model in a few significant ways that reveal information regarding the surface contour. The two primary indicators of the deviation of the sea surface slope pdf from the classic Gaussian form are expressed in the coefficients of skewness and kurtosis. The skewness is notable in the downwind direction, but negligible in the crosswind direction. If the mean and variance of the pdf derived from the Gram–Charlier series correspond to the respective values of the best-fit Gaussian pdf then $c_0 = 1/\text{sqrt}(\pi)$, $c_1 = c_2 = 0$, and Eq. (7) reduces to a Gaussian pdf with additional higher–order terms correcting for skewness and kurtosis. In this paper we do not correct for skewness and kurtosis because of the symmetry of the omnidirectional transmission. Similarly, we assume the mean slope angle is zero, although it has been found to be near zero (determined by the prevailing wind direction and material properties of the seawater) in experimental upwind and downwind measurements.

To gain a better understanding of the angular spread of a transmitted laser beam reflected from the sea surface we performed Monte Carlo simulations, launching 10^5 photons at angles of 1°–90° (with respect to the seabed surface) and computing the angle of reflection using Eqs. (4)–(6) and data from Table 2. The angle of reflection is measured from the sea surface normal. The probability density function for the sea surface slope, derived using the first term of the Gram–Charlier series that was used in our simulations, is shown in Fig. 4 for wind speeds of 3.93, 8.58, and 10.2 m/s.

A graph showing the power reception at different reflected angles as a function of incident angle for a smooth sea surface appears in Fig. 5. Below the critical angle little light is reflected by the sea surface, but above the critical angle the launched photons are totally reflected at the precise angle predicted. (Note that the transmit angle is measured from the seabed surface and not from its normal, while the reflected angle is measured from the surface normal, so that the reflected angle is the right-angle-complement of the incidence angle.) In contrast, the results of the simulations indicating the spread of reflection angles as a result of a nonsmooth sea surface are shown in Fig. 6. The wind speed is 11.5 m/s.

It is evident from Fig. 6 that when the sea surface is modeled as wavy some light is, in fact, back-reflected because of the local surface slope. The forward-reflected light propagates primarily at angles close to the right-angle-complement of the incidence angle, but considerable angular spread is encountered. In addition to the sharp contrast in the variation of the angle of arrival we observe that the angular spread results in considerable loss in received optic power when the reception angle of the receiver is limited. Photons arriving at different angles will have traversed different optical paths so multipath phenomena (e.g., pulse spread in the time domain) will also be encountered and will further reduce power reception when the receiver is pulse-gated.

A more detailed analysis of the power reception and pulse spread is beyond the scope of this paper, but clearly

Table 2. Parameters Used in Numerical Calculations[a]

Parameter	Typical Value
Extinction coefficient (m^{-1}) Clear ocean	0.1514
Temperature (°C)	10
Salinity (%)	3.5
Refractive index	1.33643
Critical angle (degrees)	48.44
Transmission wavelength (nm)	532
Optical efficiency of transmitter	0.9
Optical efficiency of receiver	0.9
Average transmitter power (W)	0.1
Pulse duration (ns)	1
Data rate (Mbit per second)	0.5
Receiver aperture area (m^2)	0.01
Laser beam divergence angle (degrees)	$\theta_0 = 68$
Transmitter inclination angles (degrees)	$\theta_{\min} = 0$ $\theta_{\max} = 68$
Dark counting rate (MHz)	1
Background counting rate (MHz)	1
Counting efficiency (%)	16
Transmitter depth-h (m)	20
Receiver depth-x (m)	20

[a]From [17,26,27].

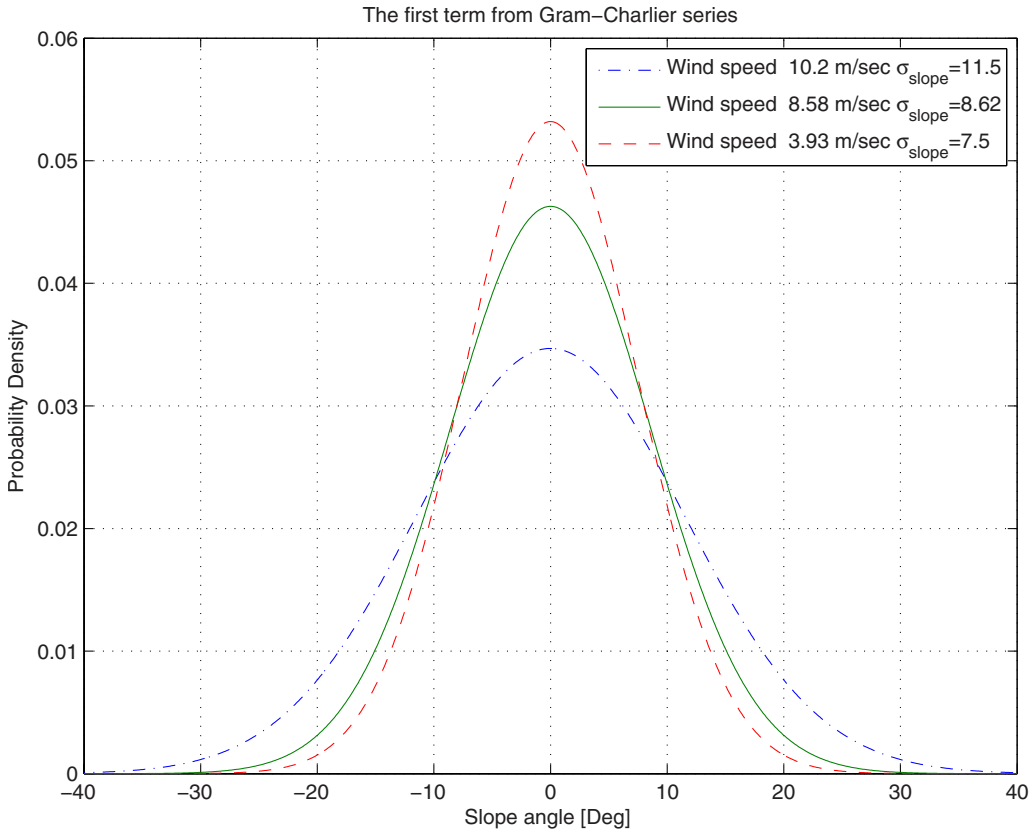

Fig. 4. (Color online) Graph showing probability density function of surface slope angle for three wind speeds.

large receiver apertures and fields-of-view are indicated as a means for mitigating the received power loss caused by the angular spread of the light reflected from a wavy sea surface.

D. Received Signal in a Reflective Communication Link (No Wave)

In Fig. 2, sensor nodes are on the seabed or floating with buoyancy control, so when the transmitter is at depth h the illuminated annular surface with equal power density at depth x is given by

$$A_{\text{ann}} = 2\pi(h+x)^2[1-\cos(\theta_{\max})-1+\cos(\theta_{\min})] = 2\pi(h+x)^2[\cos(\theta_{\min})-\cos(\theta_{\max})]. \quad (9)$$

Equation (9) describes the annular area taken from a sphere of radius $(h+x)$ that would have uniform power density in free space.

If we model the ocean–air surface as smooth then $\theta = \theta_i$, and we can derive the link budget for the sensor-to-sensor link as follows: using the variables defined in Eq. (3), we express the auxiliary function

$$f_{R\_\text{ref}}(\theta) = \frac{P_T\cos(\theta)}{A_{\text{ann}}}\begin{cases}\eta_T\eta_R\exp\left\{-c(\lambda)\left[\dfrac{h+x}{\cos(\theta)}\right]\right\}\dfrac{1}{2}\left\{\left[\dfrac{\tan(\theta_t-\theta)}{\tan(\theta_t+\theta)}\right]^2+\left[\dfrac{\sin(\theta-\theta_t)}{\sin(\theta+\theta_t)}\right]^2\right\}, & \theta_{\min}\le\theta<\theta_C \\ \eta_T\eta_R\exp\left\{-c(\lambda)\left[\dfrac{h+x}{\cos(\theta)}\right]\right\}, & \theta_c\le\theta<\theta_{\max}\end{cases}, \quad (10)$$

and calculate the received power as

$$P_{R\_\text{ref}}(\theta) = \int_{\text{Rec aper area}}\int f_{R\_\text{Ref}}(\theta)da. \quad (11)$$

At the plane of the receiving sensor, node coverage is provided within an annular area bounded by radii $(h+x)\tan(\theta_{\min})$ and $(h+x)\tan(\theta_{\max})$. Equation (11) can be simplified on the assumption that the receiver aperture is small relative to $(h+x)$, yielding the approximate received power as

$$P_{R\_\text{ref}}(\theta) \approx A_{\text{Rec}}f_{R\_\text{ref}}(\theta). \quad (12)$$

The reflective communication link provides the foundation for a powerful broadcast network. A single transmitting sensor node will communicate with a number of sen-

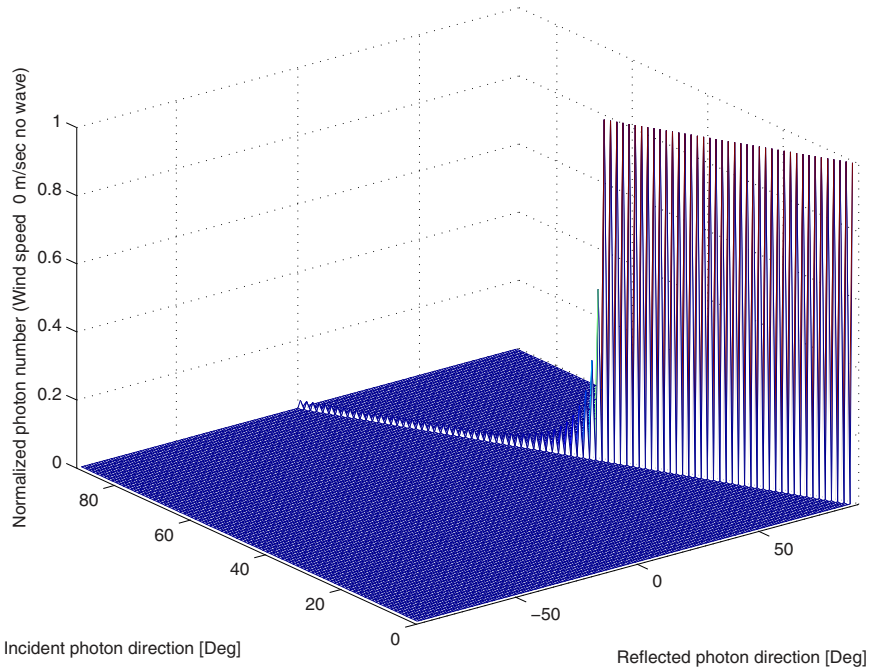

Fig. 5. (Color online) Graph showing angular distribution of power reception resulting from reflection from a smooth sea surface. Incident photon direction is measured from seabed surface, reflected photon direction is measured from sea-surface normal.

sor nodes, determined by the sparsity of the sensor node dispersion. Each receiving sensor node will be able to relay the received signal, using its transmitter, to a further population of nodes. Hence, by multiple hops, the signal can propagate long distances despite the limitations on the range of each reflective communication link. The point-to-multipoint nature of the link yields a reliable network without a single point of failure or bottleneck. Furthermore, in contrast to acoustic communications, optical communication networks can operate in full duplex and with multiple carrier frequencies. Multiple carriers would increase the payload on each sensor node, but throughput could be greatly enhanced.

4. BIT ERROR RATE

The simplest and most widespread modulation technique in FSO is intensity modulation in the form of On–Off keying (OOK). The detection method is direct detection. In our NLOS sensor network the harsh underwater environment has forced us to employ very short, high-energy pulses as our data-carrying medium. The pulse intensity

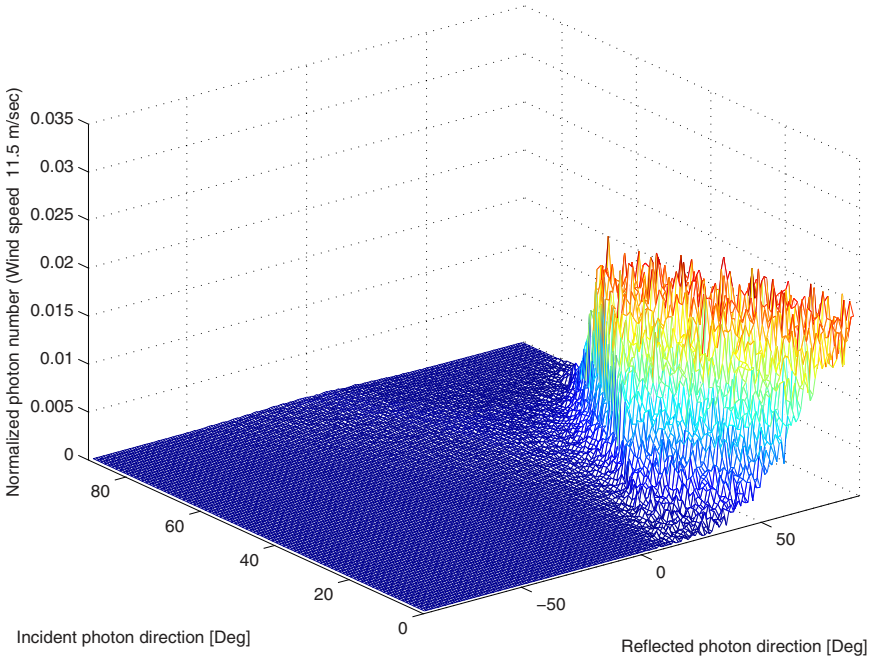

Fig. 6. (Color online) Graph showing angular distribution of power reception resulting from reflection from a simulated wavy sea surface. Incident photon direction is measured from seabed surface, reflected photon direction is measured from sea-surface normal.

is assumed much higher than any background illumination, so we do not detail the precise scenario in terms of sun zenith angle, etc. Stringent time synchronization would be necessary to operate this pulse-gated regime.

The detector is in the form of a silicon photomultiplier (SiPM) matrix [29,30]. SiPMs are built from avalanche photodiode arrays on a common substrate. Each element operates in Geiger mode and is decoupled from the neighboring cells by a quenching resistor. In common with traditional photomultiplier tubes (PMT), single photons can be detected and gains are around 10^6, but the supply voltage can be as low as 25 V, which is an order of magnitude less than for traditional PMTs. We assume that all the cells are synchronized and the detectors are modeled as photon counters. The accepted stochastic model for coherent photon arrival in photon counters is the Poisson distribution, where the photon arrival rate during the gated receiver slot of duration T is given by

$$r_s = \frac{1}{T}\left(\frac{P_R}{R_D}\right)\frac{\eta_D}{h\nu}, \tag{13}$$

where R_D is the data rate, η_D is the detector counting efficiency, P_R is P_{R_ref} or P_{R_los}, h is Plank's constant, and ν is the frequency of the photon, so that $h\nu$ is the photon energy. The BER is given by

$$P_e = P(\mathrm{one})\int_{-\infty}^{V_t} P(\xi|\mathrm{one})d\xi + P(\mathrm{zero})\int_{V_t}^{\infty} P(\xi|\mathrm{zero})d\zeta, \tag{14}$$

and assuming equiprobable transmissions of binary "1" and "0," this leads to the following expression for the BER:

$$\mathrm{BER} = 0.5\left[\sum_{n=1}^{N_{\mathrm{TH}}}\frac{(r_1T)^n\exp(-r_1T)}{n!}\right] + 0.5\left[\sum_{n=1+N_{\mathrm{TH}}}^{N_{\max}}\frac{(r_0T)^n\exp(-r_0T)}{n!}\right], \tag{15}$$

where $r_1=r_d+r_{bg}+r_s$ and $r_0=r_d+r_{bg}$, and where N_{TH} is the threshold count between "0" and "1," and r_d and r_{bg} represent the sources of additive noise due to dark counts and background illumination, respectively. If we assume a large number of photons then according to the central limit theorem the BER can be approximated by

$$\mathrm{BER} = \frac{1}{2}\,\mathrm{erfc}\left[\frac{r_1T - r_0T}{\sqrt{2}(\sqrt{r_1T}+\sqrt{r_0T})}\right], \tag{16}$$

where

$$\mathrm{erfc}(\psi) = \frac{2}{\sqrt{\pi}}\int_{\psi}^{\infty}\exp(-\gamma^2)\mathrm{d}\gamma. \tag{17}$$

5. NUMERICAL EXAMPLE

To assess the feasibility of a NLOS optical link as described above we performed numerical simulations. The values of the parameters are given in Table 2. We assume the sensors are all deployed at a depth of 20 m in clear ocean. Using Eq. (13) we calculate the expected number of received photons as a function of sensor node separation for the reflective channel. In Fig. 7 we show these results graphically and add the parallel results for a LOS channel for comparison. Using Eq. (16) we compute the expected BER as a function of sensor node separation for

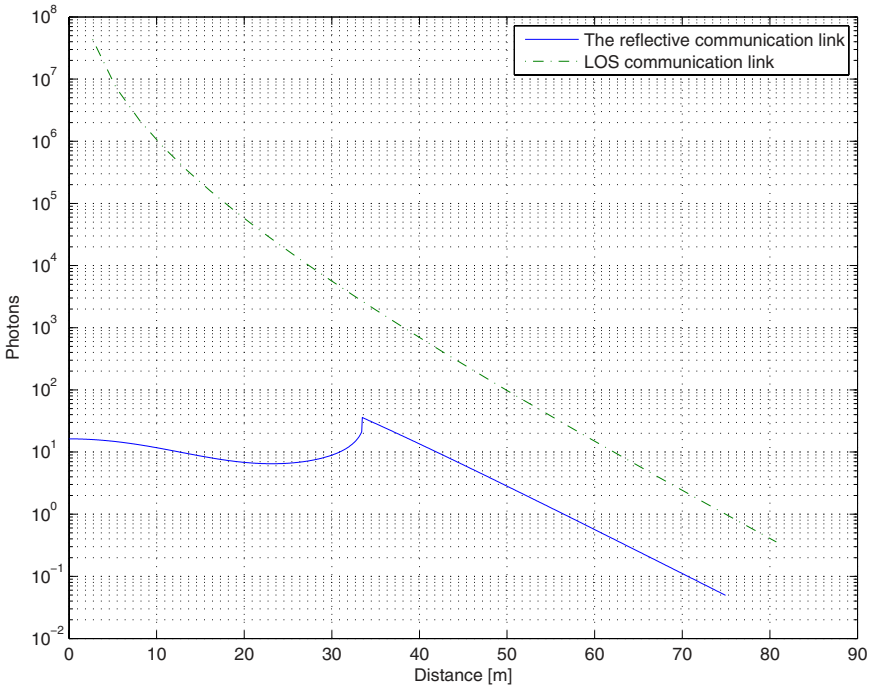

Fig. 7. (Color online) Graph showing number of received photons as a function of sensor node separation.

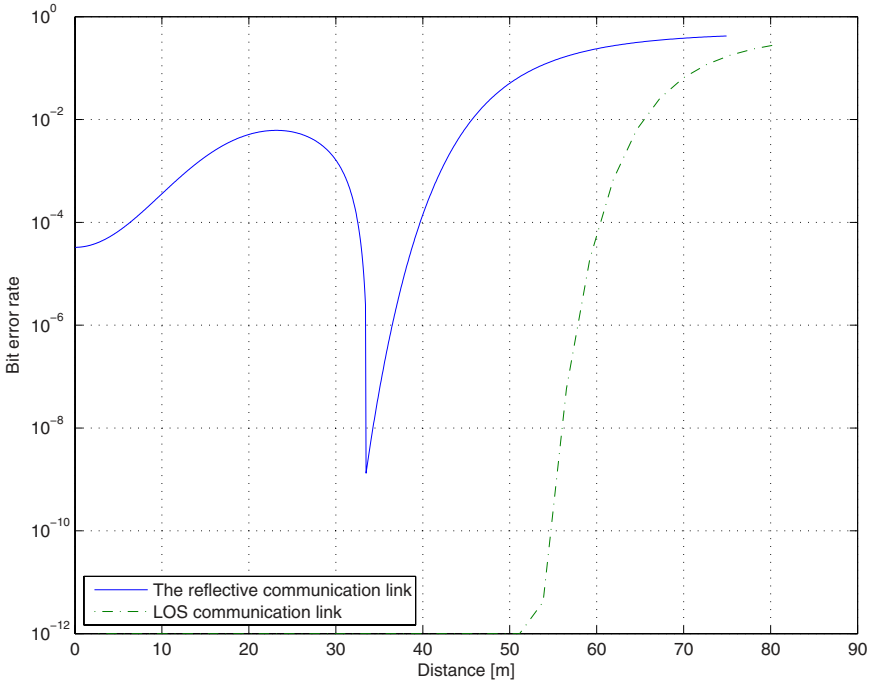

Fig. 8. (Color online) Graph showing BER as a function of sensor node separation

the reflective channel. In Fig. 8 these results are shown in a graph and the parallel results for a LOS channel are added for comparison.

It is evident from Fig. 7 that a single LOS underwater link using a pulse modulated laser transmitter and a SiPM detector array in the receiver results in a considerably higher photon count for a given sensor node separation than does a NLOS link. For instance, for a node separation of 30 m, 6,000 photons would be received from a signal in a LOS link, while only 9 would be received in a reflective link where the transmitter depth is 20 m and the receiving nodes are also at a depth of 20 m. However, if a single point-to-point link were to fail the transmitted signal would be lost, while in the NLOS underwater sensor network solution a number of nodes would be expected to receive the signal. Even in the severe case of the failure of several nodes, with sufficient node redundancy there would still be additional nodes that could relay the signal farther.

We observe an interesting phenomenon in which the number of received photons falls with node separation until a point (at ≈25 m) when the photon count increases, peaks, and falls again. We attribute this to the interplay of increased attenuation with optical path on the one hand, and increased reflectivity when the incidence angle at the ocean–air surface is greater on the other hand. Beyond some distance the attenuation dominates and the reflective link performs in a way similar to that of the LOS link. The resultant BER is affected dramatically.

In Fig. 8 we see that BER values of 10^{-4} are obtained for the NLOS reflective link when the node separation is 40 m, while a BER of 10^{-4} could be achieved in a LOS link when the node separation is 60 m. This leads us to conclude that some coding or network protocol solution would be necessary to render the NLOS link viable in an underwater sensor network with node dispersals at the depths given in the example.

6. SUMMARY AND CONCLUSIONS

In this paper we have described a model for the LOS and NLOS photon counting bit error probability in an underwater sensor network that takes into consideration the channel characteristics and the communication system parameters. We can see that an increase in node separation increases dramatically the BER of the communication system for both configurations. The results indicate that networks of underwater sensors using laser links to serve wireless mobile users are feasible at high data rates for medium distances of up to 100 m. Many aspects of the proposed NLOS underwater sensor network remain to be investigated, including rigorous modeling of the reflective nature of the ocean–air surface and a study of achievable bit rates. However the fundamental concept has been shown to be feasible and the range limitations of underwater FSO can be combatted by applying a multi-hop broadcasting network paradigm. Further work modeling multiple scattering in different oceanic channels and ocean surface roughness as well as considering solar radiance penetration should refine the analysis and yield more accurate numerical results.

REFERENCES

1. T. D. Dickey, "Emerging ocean observations for interdisciplinary data assimilation systems," J. Mar. Syst. **40–41**, 5–48 (2003).
2. N. Ehrich Leonard, D. A. Paley, F. Lekien, R. Sepulchre, D. M. Fratantoni, and E. Russ, "Collective motion, sensor networks, and ocean sampling," Proc. IEEE **95**, 48–74 (2007).
3. J. Heidemann, W. Ye, J. Wills, A. Syed, and Y. Li, "Research challenges and applications for underwater sensor networking," in *Proceedings of IEEE Wireless Communications and Networking Conference, WCNC* (IEEE, 2006) pp. 228–235.

4. J. Partan, J. Kurose, and B. N. Levine, "A survey of practical issues in underwater networks," in *Proceedings of the First ACM International Workshop on Underwater Networks, WUWNet* (ACM, 2006), pp. 17–24.
5. R. Szewczyk, E. Osterweil, J. Polastre, M. Hamilton, A. Mainwaring, and D. Estrin, "Habitat monitoring with sensor networks," Commun. ACM **47**, 34–40 (2004).
6. I. F. Akyildiz, D. Pompili, and T. Melodia, "Underwater acoustic sensor networks: research challenges," Ad Hoc Networks **3**, 257–279 (2005).
7. C. Detweiller, I. Vasilescu, and D. Rus, "An underwater sensor network with dual communications, sensing and mobility," in *Proceedings of IEEE Oceans Conference 2007—Europe* (IEEE, 2007), 4302445.
8. V. Rodoplu and M. K. Park, "An energy-efficient MAC protocol for underwater wireless acoustic networks," in *Proceedings of Marine Technology Society/IEEE Oceans Conference 2005* (IEEE, 2005), 1639918.
9. I. Vasilescu, K. Kotay, D. Rus, P. Corke, and M. Dunbabin, "Data collection, storage and retrieval with an underwater sensor network," in *Proceedings of the 3rd International Conference on Embedded Networked Sensor Systems*, (ACM, 2005), pp. 154–165.
10. F. Hanson and S. Radic, "High bandwidth underwater optical communication," Appl. Opt. **47**, 277–283 (2008).
11. N. Farr, A. Chave, L. Freitag, J. Preisig, S. White, D. Yoerger, and P. Titterton, "Optical modem technology for seafloor observatories," in *Proceedings of IEEE Oceans Conference 2005* (IEEE, 2005), pp. 928–934.
12. D. Kedar and S. Arnon, "Non-line-of-sight optical wireless sensor network operating in multiscattering channel," Appl. Opt. **45**, 8454–8461 (2006).
13. D. Kedar, "Multiaccess interference in a non-line-of-sight ultraviolet optical wireless sensor network," Appl. Opt. **46**, 5895–5901 (2007).
14. D. Kedar and S. Arnon, "Optical plankton: an optical oceanic probing scheme," J. Appl. Remote Sensing **1**, 013541 (2007).
15. N. G. Jerlov, *Marine Optics* (Elselvier, 1976).
16. R. P. Bukata, J. H. Jerome, K. Y. Kondratyev, and D. V. Pozdnyakov, *Optical Properties and Remote Sensing of Inland and Coastal Waters* (CRC Press, 1995).
17. J. H. Smart, "Underwater Optical Communication systems Part 1: variability of water optical parameters," in *Proceedings of IEEE Military Communications Conference, MILCOM* (IEEE, 2005), 1605832.
18. T. J. Petzold, "Volume scattering functions for selected ocean waters," Paper SIO Reference 72-78, Scripps Institute of Oceanography (1972).
19. X. Quan and E. S. Fry, "Empirical equation for the index of refraction of seawater," Appl. Opt. **34**, 3477–3480 (1995).
20. NOAA's National Data Buoy Center, http://www.ndbc.noaa.gov/wave.shtml.
21. K. E. Steele and M. D. Earle, "Directional ocean wave spectra using buoy azimuth, pitch and roll derived from magnetic field components," IEEE J. Ocean. Eng. **16**, 427–433 (1991).
22. S. Premoze and M. Ashikhmin, "Rendering natural waters," Comput. Graph. **20**, 189–199 (2001).
23. M. Onorato, A. R. Osborne, M. Serio, L. Cavaleri, C. Brandini, and C. T. Stansberg, "Observation of strongly non-Gaussian statistics for random sea surface gravity waves in wave flume experiments," Phys. Rev. E **70**, 167302 (2004).
24. G. W. Petty and K. B. Katsaros, "The response of the SSM/I to the marine environment. Part II: a parameterization of the effect of the sea surface slope distribution on emission and reflection," J. Atmos. Ocean. Technol. **11**, 617–628 (1994).
25. S. Arnon, "Optical wireless communication," in *Encyclopedia of Optical Engineering*, R. G. Driggers, ed. (Marcel Dekker, 2003) pp. 1866–1886.
26. C. Cox and W. Munk, "Slopes of the sea surface deduced from photographs of sun glitter," Bull. Scripps Inst. Oceanogr. **6**, 401–488 (1956).
27. W. J. Plant, "A new interpretation of sea-surface slope probability density functions," J. Geophys. Res. **108**, pp. 11-1–11-4 (2003).
28. J. A. Shaw and J. H. Churnside, "Scanning-laser glint measurements of sea-surface slope statistics," Appl. Opt. **36**, 4202–4213 (1997).
29. P. Eraerds, M. Legre, A. Rochas, H. Zbinden, and N. Gisin, "SiPM for fast photon-counting and multiphoton detection," Opt. Express **15**, 14539–14549 (2007).
30. H.-G. Moser, "Silicon photomultipliers, a new device for low light level photon detection," in *AIP Conference Proceedings, Calorimetry in High Energy Physics: XII International Conference* (AIP, 2006), pp. 867, 98–105.